Why Are There Upwellings on the Northern Shelf of Taiwan under Northeasterly Winds?

YU-LIN CHANG

Program in Atmospheric and Oceanic Sciences, Princeton University, Princeton, New Jersey, and Department of Earth Sciences, National Taiwan Normal University, Taipei, Taiwan

LIE-YAUW OEY

Program in Atmospheric and Oceanic Sciences, Princeton University, Princeton, New Jersey

CHAU-RON WU AND HUNG-FU LU

Department of Earth Sciences, National Taiwan Normal University, Taipei, Taiwan

(Manuscript received 24 August 2009, in final form 27 January 2010)

ABSTRACT

Upwellings are observed on the northern shelf of Taiwan during northeasterly winds. Analytical and realistic numerical models are used to explain how vertical motions are created by divergence and convergence produced by wind acting on the vorticity field of two strong jets: the Kuroshio and the Taiwan Warm Current. The seaward increase in cyclonic vorticity near the Kuroshio's western edge favors a stronger Ekman transport away from the jet, producing upwelling at the shelfbreak under a northeasterly wind. A similar mechanism for generating vertical motions is found across the Taiwan Warm Current. The numerical model results indicate that the vorticity effects can account for up to 30%–50% of the total variation in the surface Ekman transport. Except during summer's weak southwesterlies, northeasterly wind is dominant over the East China Sea, suggesting that the vorticity effects may be prominent in the observed shelfbreak upwelling in nonsummer months.

1. Introduction

The shelf region off the northern coast of Taiwan is sandwiched between the Kuroshio and the Taiwan Warm Current (TWC; Figs. 1, 2); the regional circulation is therefore expected to be strongly influenced by these two currents. The Kuroshio flows along the eastern coast of Taiwan and turns northeastward as it collides with the continental shelf of East China Sea. The Taiwan Warm Current flows northeastward from the South China Sea through the Taiwan Strait and enters the East China Sea. The TWC is stronger along the western coast of Taiwan. The mean speed of the TWC is about 0.40 m s^{-1} according to the analysis of shipboard ADCP data from 1999 to 2001 (Wang et al. 2003). A composite shipboard ADCP current velocity from 1991 to 2000 also indicated that the TWC strengthened along the western coast of Taiwan (Liang et al. 2003).

Using hydrographic and chemical observations, Liu et al. (1992b) observed an abrupt temperature drop off the northern coast of Taiwan after the prevailing wind changed from southwesterly to northeasterly. The authors noted that upwelling brought nutrient-rich Kuroshio water onto the continental shelf. Wong et al. (2004) also reported upwelling at the shelf edge based on temperature and nitrate observations along a transect (their section E) on the northern shelf of Taiwan (near the section shown in Fig. 1). The authors did not examine the wind conditions, but we checked the wind at Pen-Chia Yu (PCY) (Fig. 2) and found that, of the five cross-shelf surveys, the southern three sections, C, D, and E (27°–25°N), were surveyed during northeasterly winds (approximately 8–18 May 1996; section E was near the section shown in Fig. 2). The authors noted that ''shoreward intrusion across the shelf was more extensive in the southern part.'' In both of these works, because of the orientation of the

Corresponding author address: Lie-Yauw Oey, Program in Atmospheric and Oceanic Sciences, Sayre Hall, Princeton, NJ 08544. E-mail: lyo@princeton.edu

DOI: 10.1175/2010JPO4348.1

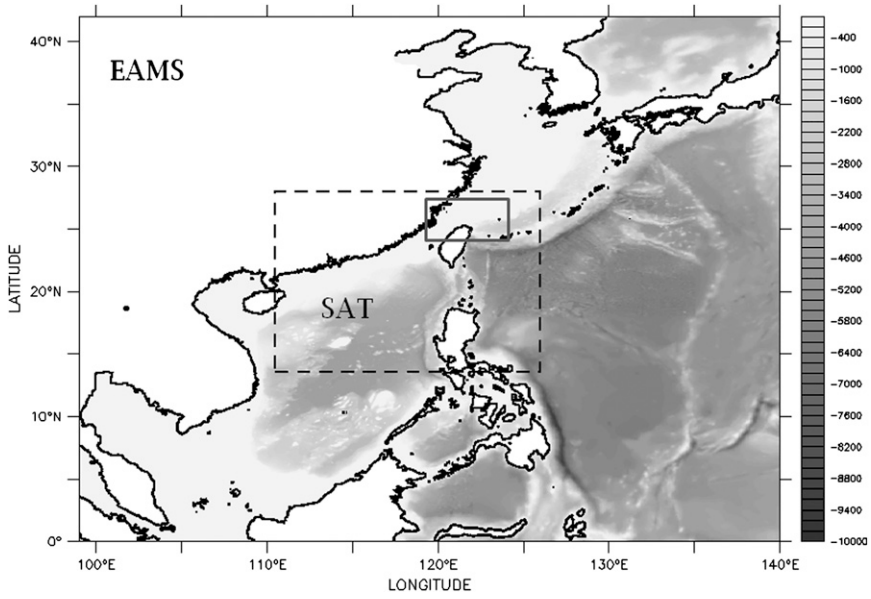

FIG. 1. EAMS and SAT (dashed box) model domains. Grayscale is the ocean topography in meters. The solid box is the analysis region for this study, as shown in Fig. 2.

East China Sea shelf north of Taiwan, northeasterly winds correspond to downwelling-favorable winds and the observed upwelling is puzzling. Chen and Wang (2006) also reported upwelling and downwelling events over the shelf near the edge of TWC but away from the coast. The authors did not examine the contemporaneous wind field; data shown later indicate that the wind was also from the northeast during their cruise. Their observations suggest that the TWC played a role in the observed upwelling and downwelling.

In the case of the East China Sea, upwellings are observed on the shelf and shelf edge away from coastal divergence [positive and negative (or convergence) same below] zone. However, winds acting on the vorticity fields of strong ocean currents such as the Kuroshio and the TWC can produce divergence near the surface (Niiler 1969). The objective of this study is to investigate Niiler's mechanism, specifically upwellings during downwelling-favorable winds as observed by Liu et al. (1992b) and Wong et al. (2004) and vertical motions over the shelf near the TWC as observed by Chen and Wang (2006). Additionally, we will use temperature time series at the LongTung buoy (Fig. 2) near the northeastern shelf edge of Taiwan to formulate and check our theory. We will explain the phenomenon by taking into account the effect of the Kuroshio and TWC on the shelf circulation induced by northeasterly winds.

In addition to wind forcing on the ocean's vorticity, other mechanisms can also generate upwelling. Kuroshio meanders and/or frontal eddies may produce intense vertical motions at the shelf edge (Ito et al. 1995; Yanagi et al. 1998; Wu et al. 2008, and references therein). Interaction of the strong current with topography also produces vertical motions (Hsueh et al. 1992; Stern and Austin 1995), and so does cooling in combination with the joint effect of baroclinicity and relief (JEBAR) effects (Oey et al. 2010). Wind stress curl can be important over long time scales in modulating the strength of upwelling over the northern shelf of Taiwan (Chang et al. 2009). The present study focuses solely on the effects of strong jets in modifying the surface Ekman transports of a spatially uniform wind field.

The paper is organized as follows: The observations (section 2) and the numerical model (section 3) are described first. Section 4 describes a simple analytical model to explain the LongTung buoy observation. Section 5 uses the numerical model to explain Chen and Wang's (2006) observations. The conclusions are in section 6.

2. Observations

Liu et al. (1992b) collected their data during three cruises on 1–6 August, 18–23 September, and 20–25 October 1990, using a conductivity–temperature–depth (CTD) rosette to obtain temperature, salinity, and water samples. Wong et al.'s (2004) cruises were from 2 through 15 May 1996 and covered the East China Sea from 25° to 30°N. Temperature and nitrate data were collected along five cross-shelf transects, the southernmost of which cut across the northern shelf of Taiwan

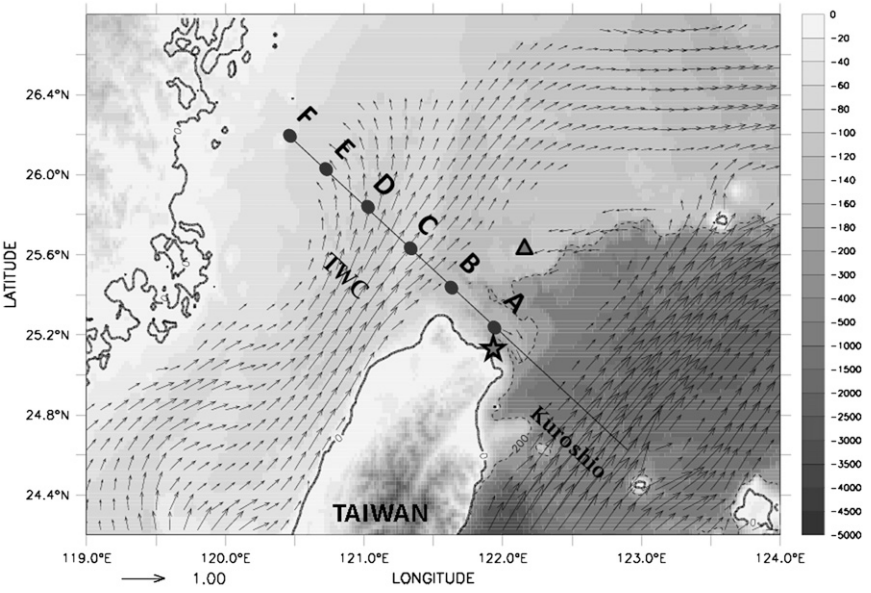

FIG. 2. Study region with averaged flow filed in August 2001. Velocities with speeds >0.2 m s^{-1} are shown. The dashed line is the 200-m isobath, the star indicates the location of LongTung buoy, the triangle shows the PCY wind station, dots show the location of the observation from stations A–F in Chen and Wang (2006), the black solid line is the transect used for analysis, and the shading shows topography in meters.

and extended onto the western edge of the Kuroshio (near the section shown in Fig. 2). Chen and Wang (2006) conducted their cruise from 27 to 28 August 2001, also using CTD. Chen and Wang's station locations from A to F are plotted in Fig. 2.

Wind data used for the numerical model are from the National Aeronautics and Space Administration (NASA) Quick Scatterometer (QuikSCAT)–National Centers for Environmental Prediction (NCEP) ocean surface wind archive. These wind data are derived from spatial blending of high-resolution satellite data (Seawinds instrument on the QuickSCAT satellite) and the NCEP global reanalysis using a temporal resolution of 6 h and a spatial resolution of 0.5° × 0.5°. For analysis and checking purposes, wind data are also obtained from a weather station PCY located at 25.63°N, 122.07°E (triangle in Fig. 2) of the Taiwan Central Weather Bureau. Sea surface temperature (SST) was also obtained at the LongTung buoy at 25.1°N, 121.92°E (star in Fig. 2). The buoy is approximately 1 km off the coast and is near the location where upwelling was observed by Liu et al. (1992b, their Fig. 4b) and Wong et al. (2004, their Fig. 2).

3. The numerical model

The Seas Around Taiwan (SAT) model for this study is constructed according to the Princeton Ocean Model (POM; Mellor 2004). The Princeton Ocean Model is based on hydrostatic primitive equations in sigma coordinates. At the open boundaries, the SAT model derives its boundary conditions from a larger-scale East Asian Marginal Seas (EAMS; Hsin et al. 2008) model (Fig. 1). Thus, transports normal to the boundary are specified from EAMS, whereas the vertical structures of the currents (with zero transport) are specified using radiation conditions. The velocity component tangential to the boundary, as well as turbulence kinetic energy and length scale, are specified using a one-sided advection scheme at outflow grids and are set to zero at inflow. The temperature and salinity are similarly advected during outflow but are specified with EAMS values at inflow grids. Because of the staggered C grid used and with normal transports specified, boundary elevation is not an active variable, and it is set equal to its immediate interior value. Details of the EAMS model are given in Hsin et al. (2008). Briefly, EAMS model extends from 0° to 42°N and from 99° to 140°E. The horizontal resolution is 1/8°, and it has 26 vertical sigma levels. The EAMS model is forced by 6 hourly QuikSCAT–NCEP wind data, and it is nested within a 1/4° × 1/4° × 26 sigma-level North Pacific model using similar nesting boundary conditions described above for the SAT model. The simulation period is from 1980 to 2005.

The SAT model domain extends from 13.5° to 28°N and from 110.5° to 126°E (dashed box in Fig. 1). The

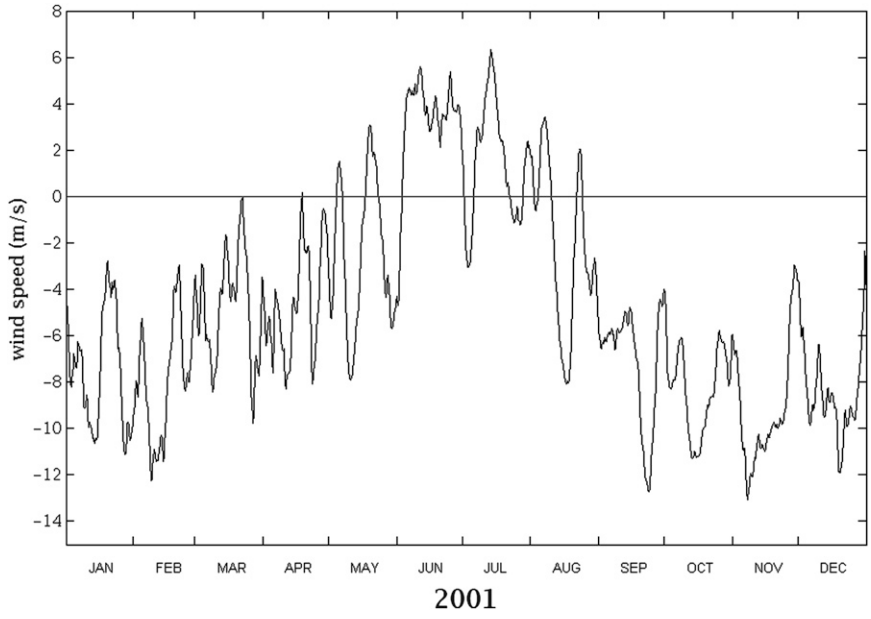

FIG. 3. The 5-day running averaged QuikSCAT wind velocity normal to the transect shown in Fig. 2 during 2001: positive is southwesterly and negative is northeasterly.

horizontal grid size is 1/20°, and there are 26 sigma levels in the vertical. The SAT model was initialized by the temperature and salinity fields of the EAMS model outputs for January 1999 and was then subjected to climatologically forcing for 1 yr. After this spinup period, the SAT model was forced with QuikSCAT–NCEP wind data from 2000 through 2005. A detailed description of the SAT model has been given by Wu et al. (2008). The analysis region for this study is shown in Fig. 1 (solid box), within which the simulated results for August–September 2001 are used.

In addition to Liu et al.'s (1992b) data from August to October 1990 and Wong et al.'s (2004) observations in May 1996, Chen and Wang's (2006) observations of upwelling on the northern shelf of Taiwan in August 2001 were also during a period of northeasterly winds (see later). These latter dates are within our model simulation dates. We will therefore explain the upwelling event during Chen and Wang's (2006) cruise. Figure 2 shows the simulated flow field. Vectors are surface currents averaged over August 2001 but are shown for velocity greater than 0.2 m s^{-1}; the positions of Kuroshio and TWC are clearly seen. The black solid line shows Chen and Wang's (2006) cruise transect, and symbols indicate the locations of observation from stations A–F. We extend their transect to also include a portion of the Kuroshio. Upwellings were observed on the shelf near the two strong currents (Liu et al. 1992b; Wong et al. 2004; Chen and Wang 2006).

The East Asian monsoon wind is southwesterly during summer and northeasterly during winter. Figure 3 shows the 5-day running averaged QuikSCAT wind velocity normal to the track (solid line in Fig. 2). Positive values indicate southwesterly wind, and negative values indicate northeasterly wind. In 2001, the wind was northeasterly from January to May and became southwesterly from the middle of May through approximately the middle of August. The wind reversed to become northeasterly from the middle of August through the end of the year. Therefore, the observed upwelling by Chen and Wang (2006) in late August 2001 was under the onset of ''winter'' monsoon; the wind condition was similar to that observed during Liu et al.'s (1992b) and Wong et al.'s (2004) cruises.

4. Shelf-edge upwelling: The LongTung measurement

The LongTung buoy is located off the northeastern extremity of Taiwan at the western edge of the Kuroshio; its temperature is expected to be influenced by the interaction of wind with the vorticity field of the Kuroshio. We explore this possibility using a simple model, which will also serve as the basis for a more detailed examination using the numerical model in section 5.

The heat equation is

$$\partial T/\partial t + \mathbf{u} \cdot \nabla T = \partial Q/\partial z, \tag{1}$$

where T is (potential) temperature; t is time; $\mathbf{u}$ is the velocity with cross-shelf x (positive offshore), along-shelf

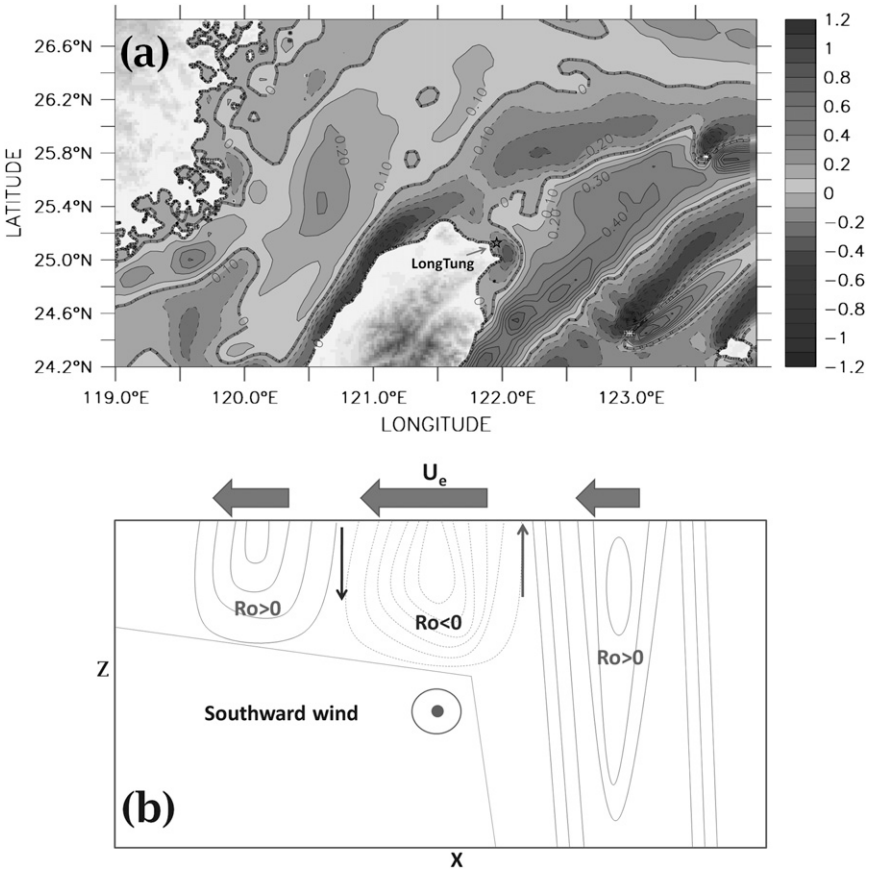

FIG. 4. (a) Surface nondimensional vorticity $R_{os} = \zeta_s/f_0$ averaged over the study period August–10 Sep 2001 from the model. (b) Schematic diagram of surface Ekman transport U_e and vertical velocity (vertical arrows) during southward wind according to Eq. (4).

y (positive poleward) and vertical z (positive upward with $z = 0$ at the sea surface) components (u, v, w); and Q is the vertical heat flux. Linearize (1) about a time-independent background field $T_0(x, z)$; integrate from $z = -\delta_E$ to $z = 0$, where δ_E is the Ekman depth; and assume that $\mathbf{u}$ is solely due to the (kinematic) wind stress $\boldsymbol{\tau}_0 = (\tau_0^x, \tau_0^y)$, and we obtain

$$\partial T/\partial t = (\mathbf{k} \times \boldsymbol{\tau}_0) \cdot \nabla T_0/(f\delta_E) - \mathbf{k} \cdot [\nabla \times (\boldsymbol{\tau}_0/f)](\Delta T/\delta_E) + Q_s - \alpha_N T, \quad (2a)$$

where $\mathbf{k}$ is the upward (z) unit vector, $f = f_0 + \zeta_s$ (f is assumed >0), f_0 is the Coriolis parameter $\approx 6.2 \times 10^{-5}$ s^{-1} at 25.5°N, ζ_s $[=(\partial v/\partial x - \partial u/\partial y)|_{z=0}]$ is the vertical component of the relative vorticity at the surface, $\Delta T = \delta_E(\partial T_0/\partial z)[\approx T_0(z = 0) - T_0(z = -\delta_E)]$, and $\alpha_N T$ approximates Q at $z = -\delta_E$ as a Newtonian cooling term with constant coefficient α_N. In deriving (2a), ∇T_0 is assumed to be independent of z across the thin Ekman layer, and the inclusion of ζ_s in f_0 follows Niiler (1969).

Let the along-slope (y) scales be much larger than the cross-slope (x) scales: $\partial/\partial y \ll \partial/\partial x$. We will later verify the validity of this assumption using the numerical model. Equation (2a) then becomes, in the cross-slope vertical x–z plane (e.g., along the transect in Fig. 2),

$$\partial T/\partial t = \tau_0^y/(f\delta_E)(-\partial T_0/\partial x + \partial \zeta_s/\partial x \Delta T/f) + Q_s - \alpha_N T. \quad (2b)$$

Thus,

$$u \approx U_e/\delta_E = \tau_0^y/(f\delta_E) \quad \text{and} \quad (3a)$$

$$w \approx \partial(\tau_0^y/f)/\partial x = -(\tau_0^y/f^2)\partial \zeta_s/\partial x, \quad (3b)$$

where U_e is the surface Ekman transport; it can be written as

$$U_e = \frac{\tau_0^y}{f_0(1 + R_{os})}, \quad (4)$$

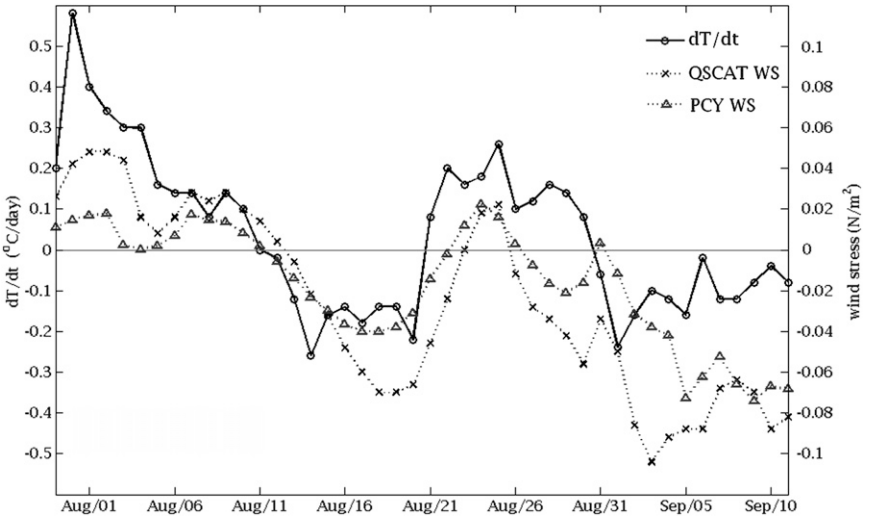

FIG. 5. Wind stresses computed from the QuikSCAT (black dashed line) and PCY (dashed line) winds and the rate of change of LongTung buoy's SST (solid line; the $\partial T/\partial$t is shifted forward by 2 days). The line separates positive and negative values.

where $R_{os} = \zeta_s/f_0$ is the surface nondimensional vorticity ($R_o = \zeta/f_0$).[1] Because of the vorticity field, surface divergences and convergences exist even if τ_0^y is spatially constant. The wind stress curl can be important over larger spatial and temporal scales (Chang et al. 2009); however, for the present study, $\nabla \times \boldsymbol{\tau}_0 = 0$ is assumed. Figure 4a plots the time-averaged R_{os} from the model and shows along-slope banded structures resulting from the Kuroshio and TWC; $R_{os} \approx O(1)$, and its effects on the Ekman transport may not be negligible. Upwelling occurs for a "southward" wind (kinematic) stress $\tau_0^y < 0$ in regions where $\partial\zeta_s/\partial x > 0$ (e.g., northeastern slope of Taiwan at the western edge of the Kuroshio; Fig. 4b), and this leads to cooling $\partial T/\partial t < 0$ [second or "vorticity" term on the rhs of Eq. (2b)]. On the other hand, the first (or "temperature gradient") term on the rhs of Eq. (2b) gives a warming tendency $\partial T/\partial t > 0$ (for $f > 0$) for the same southward wind, because $\partial T_0/\partial x > 0$ near the western edge of the Kuroshio. Assuming that, on time scales of days to weeks, $Q_s \approx$ constant and also that the Newtonian cooling term is small (these assumptions are checked later), we may use the LongTung buoy temperature measurement to check if one of these two competing processes dominates.

For inviscid response (i.e., $\alpha_N = 0$), Eq. (2b) shows that $\partial T/\partial t$ is in phase or positively correlated (out of phase, equal to π, or negatively correlated) with τ_0^y if the vorticity (temperature gradient) term dominates. The rate of change of LongTung temperature is visually found to be nearly in phase with τ_0^y; the correlation coefficient is ≈(0.5–0.76) for lags ranging from 0 to 3 days ($\partial T/\partial t$ lags τ_0^y). A nonzero α_N would tend to decrease the lag between T and τ_0^y to some value below $\pi/2$ (the corresponding lag for $\alpha_N = 0$), resulting in $\partial T/\partial t$ leading τ_0^y by the same amount. Therefore, the fact that $\partial T/\partial t$ lags τ_0^y strongly suggests that α_N is small and that the effects of mixing with subsurface water are overwhelmed by other processes. The α_N is estimated from values of the eddy diffusivity $K_H < 10^{-4}$ m^2 s^{-1} for depths deeper than the surface Ekman layer $\delta_E \approx 20$ m below the surface (but outside the bottom boundary layer) computed by the numerical model using the Mellor and Yamada (1982) level-2.5 turbulence closure scheme. Because $\alpha_N \approx K_H/\delta_E^2$, we obtain $\alpha_N < 3 \times 10^{-7}$ s^{-1}, or an e-folding time scale of about 40 days for mixing of surface and subsurface waters. The ratio of the Newtonian cooling term $\alpha_N T$ to the tendency term $\partial T/\partial t$ in (2b) is indeed small, because it is $\alpha_N/\omega < 0.1$, where $2\pi/\omega$ is the wind period ≈15–20 days (Figs. 3, 5).

Figure 5 shows the rate of change of SST at the LongTung buoy (solid line) and wind stresses computed for QuikSCAT (dashed line with X) and Peng-Chia Yu wind (dashed line with triangles). The Large and Pond (1981) formula is used to compute the wind stress, and all data have been 5-day averaged. In early August, the wind stress was positive or southwesterly. The wind became northeasterly 13–21 August, was southwesterly 22–26 August, and turned northeasterly thereafter. Figure 5 shows that the buoy SST was increasing ($\partial T/\partial t > 0$;

[1] The absolute value of R_o is the Rossby number used in theoretical analyses as a measure of inertial versus the Coriolis force i.e., $|\zeta|/f_0$.

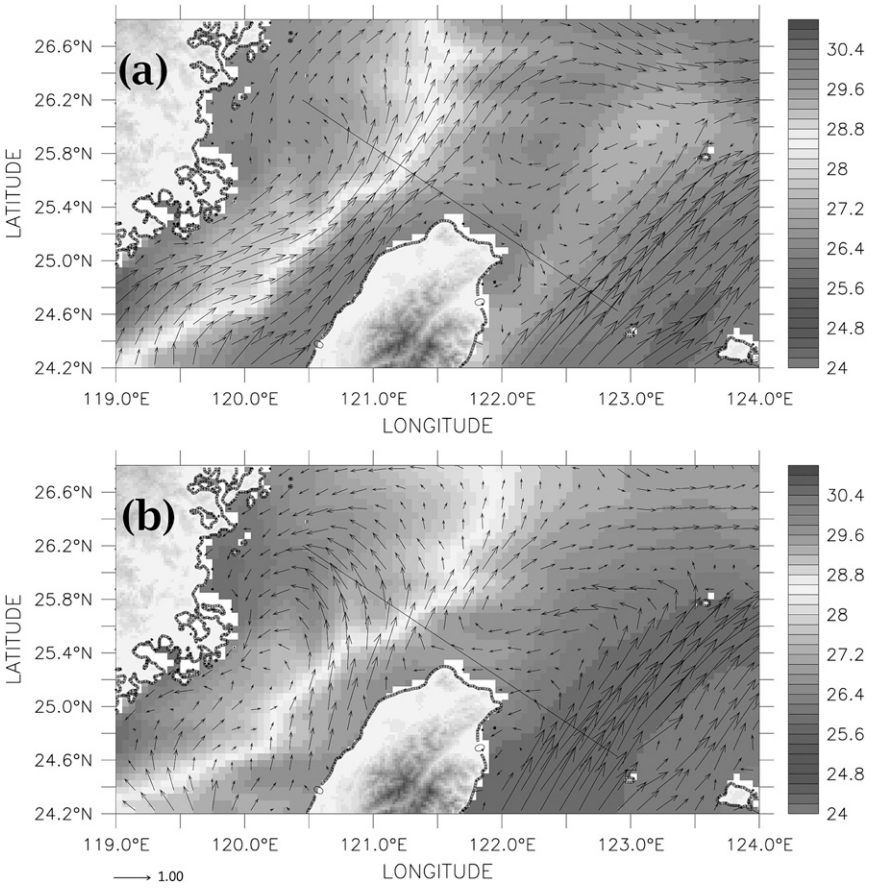

FIG. 6. Composite-modeled temperature (°C) and surface flow field during (a) southwesterly wind and (b) northeasterly wind during the study period. The black line shows the position of the track (see Fig. 2).

approximately 2 days) after the wind turned southwesterly ($\tau_0^y > 0$), and SST was decreasing ($\partial T/\partial t < 0$) when the wind was northeasterly ($\tau_0^y < 0$). The positive, nearly in-phase correlation suggests that the vorticity term dominates in Eq. (2b). There are exceptions that indicate when the temperature-gradient term was important: for example, 3–5 days near the end of August when warming ($\partial T/\partial t > 0$) coincided with a northeasterly wind ($\tau_0^y < 0$). The dominance of the temperature-gradient term results in $\partial T/\partial t$ lagging τ_0^y by π (for $\alpha_N = 0$), which likely explains the higher correlation between the observed $\partial T/\partial t$ and τ_0^y when a small lag of 2 days is used (Fig. 5).

We ascertain that Q_s was unimportant, particularly that the temperature drops were not a result of intense heat-loss events during the northeasterly winds (Fig. 5), in two ways. First, weather records for August–10 September 2001 at a station in Keelung City (northern Taiwan) obtained from the Central Weather Bureau (available online at http://www.cwb.gov.tw) were examined. These showed no cold-air outbreaks during the period. Second, simulated temperature from the SAT model (see later) in the upper 30 m at a grid near the LongTung buoy was found to display very similar warming and cooling variations (not shown). The cooling events in particular cannot be due to Q_s, because cold-air outbreaks were not included in the SAT model.

In summary, the positive, nearly in-phase correlation between the observed $\partial T/\partial t$ and τ_0^y strongly suggests that the vorticity effect in Eq. (2) dominates. Wind acting on the vorticity field is significant in producing surface divergences and convergences and hence upwelling and downwelling, which in turn affect the ocean temperature near the western edge of the Kuroshio.

5. Numerical model results

It is clear from earlier that the effects of strong shears from the Kuroshio cannot be neglected when considering the wind-driven response at the shelf edge. Here, we show that the same mechanism applies also on the northern shelf sandwiched between the Kuroshio and TWC.

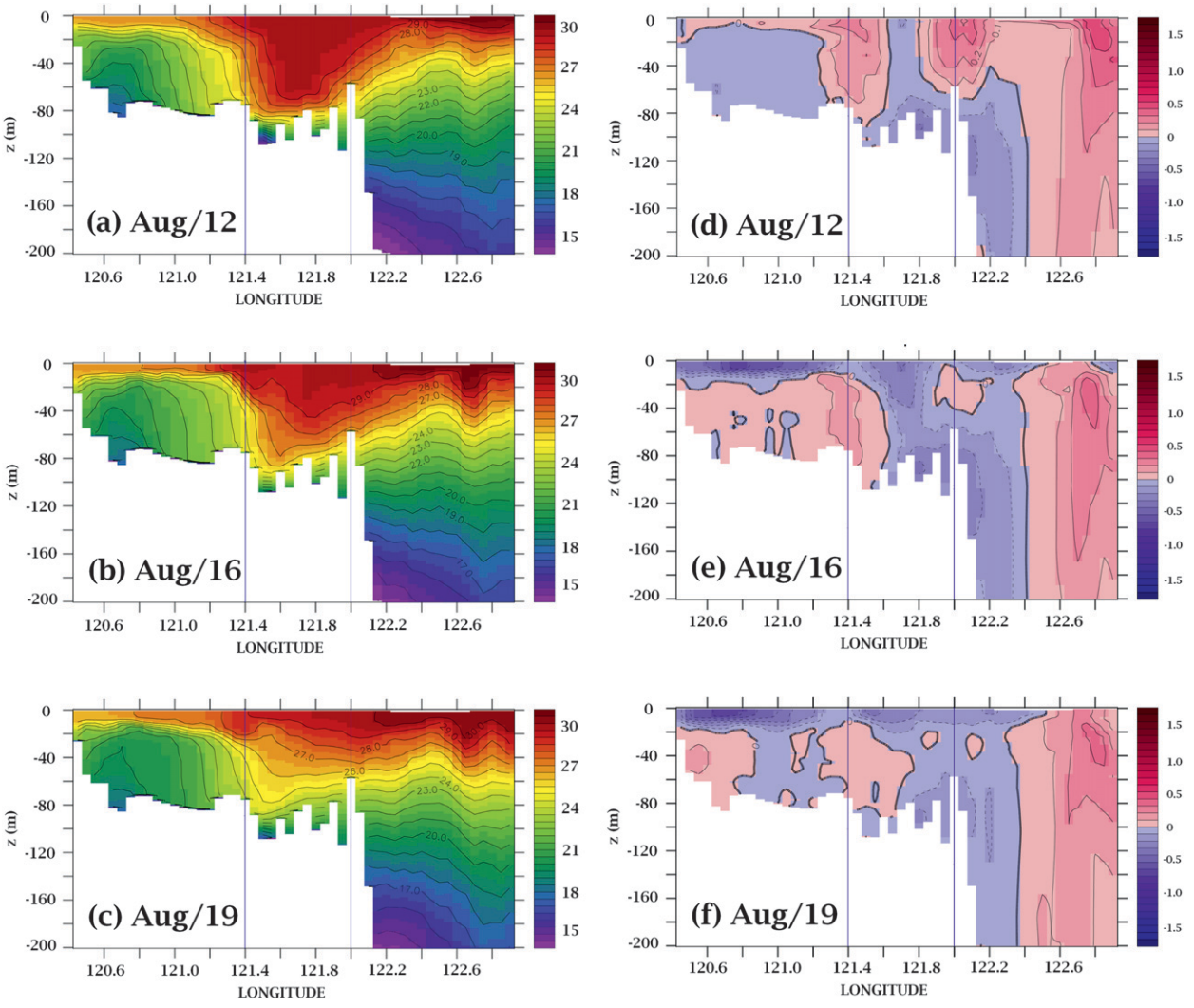

FIG. 7. Section contours of the (left) modeled temperature and (right) along-track velocity along the track shown in Fig. 2 on (a),(d) 12 Aug; (b),(e) 16 Aug; and (c),(f) 19 Aug. Blue solid lines separate, from left to right, the Taiwan Strait, northern shelf of Taiwan, and Kuroshio. The contour interval is 1°C for temperature and 0.1 m s^{-1} for the along-track velocity.

The action of wind on the vorticity fields of these two currents complicates the resulting circulation.

The modeled surface temperature and flow field were composited for southwesterly (Fig. 6a) and northeasterly (Fig. 6b) wind in August 2001. During the southwesterly wind, both Kuroshio and TWC were stronger than during northeasterly wind. The strengthening of the currents during southwesterly winds may be related to frontal intensification by downfront wind discussed by Thomas and Lee (2005), but our model resolution is too coarse for this mechanism to be fully resolved. During northeasterly wind, the coastal current along the Chinese coast reversed with the wind and the temperature was cooler along the western coast of Taiwan. On the northern shelf of Taiwan, the flow was eastward out of Taiwan Strait during the southwesterly wind; the flow was westward from Kuroshio to the shelf during the northeasterly wind.

Figure 7 shows the vertical section plots of temperature and the along-track (i.e., onshore–offshore) velocity on 12, 16, and 19 August along the transect (shown in Fig. 2). In this and other section plots later, the northern shelf (121.4°–122°E) is sandwiched between the two blue solid lines: Taiwan Strait is to the west and Kuroshio is to the east. The 12 August plot indicates the condition near the end of the southwesterly wind (Fig. 5), whereas the plots for 16 and 19 August represent the ocean responses during the northeasterly wind. Before the wind reversed on 12 August, the northern shelf of Taiwan was occupied by warm water ($T > 29$°C) in the upper 70 m. In Taiwan

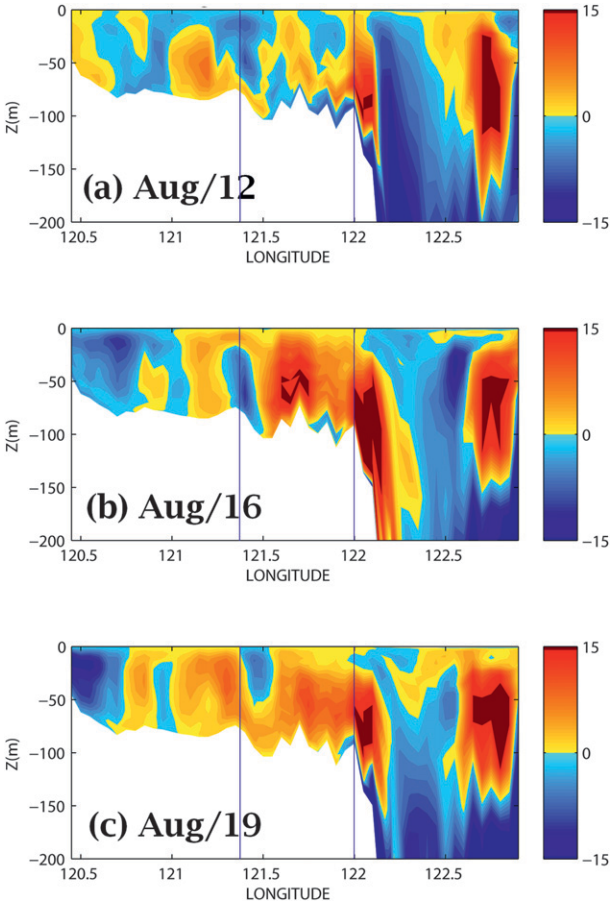

FIG. 8. Section contours of the modeled vertical velocity along the track shown in Fig. 2 on (a) 12, (b) 16, and (c) 19 Aug. Units are m day^{-1}.

Strait, the near-surface current flowed eastward out of the strait and the bottom flow was westward. Except for a narrow region of weak westward flow from 121.6° to 121.8°E, the near-surface current on the northern shelf of Taiwan was also predominately eastward and merged with the Kuroshio (Fig. 7d). During the onset of northeasterly wind, both the near-surface and bottom flows reversed directions (Figs. 7e,f). Inside the Taiwan Strait, the near-surface flow was westward, and the flow was eastward near the bottom. On the northern shelf of Taiwan, surface flow was westward from the edge of the Kuroshio to the shelf. On 16–19 August, a few days after the northeasterly wind, an upwelling can be seen from the temperature contours on the northern shelf of Taiwan (Fig. 7b), and the upwelling was fully developed on 19 August (Fig. 7c). Between 12 and 19 August, the 29°C isotherm was uplifted from a depth of $z = -70$ m to $z = -20$ m; that is, $w \approx 7$ m day^{-1}.

The vertical velocity also shows this upwelling during the onset of northeasterly wind (Fig. 8). The vertical velocity is plotted on the same days as Fig. 7. Colors separate the positive (red) and negative values (blue). On 12 August (Fig. 8a), upwelling (~120.5°E) is seen near the Chinese coast, which is consistent with the surface offshore and bottom onshore velocity plot (Fig. 7d). On 16 (Fig. 8b) and 19 August (Fig. 8c) for downwelling-favorable wind, onshore surface flow induced downwelling near the Chinese coast. By contrast, under this downwelling-favorable wind, the model shows increased upwelling on the northern shelf of Taiwan and at the shelf edge. The maximum vertical velocity reached 15 m day^{-1} on the shelf and over 40 m day^{-1} at the shelf edge. The latter upwelling agrees well with the analysis at the LongTung buoy presented previously (section 4 and Fig. 5).

We now explain why the downwelling-favorable wind can produce upwelling on the northern shelf of Taiwan; we will attempt to connect the model results with Chen and Wang's observation. The left panel of Fig. 9 shows the velocity normal to the track on the same days as Fig. 7. The northern shelf of Taiwan is sandwiched between two strong jets (fronts, Fig. 9a); to the west is the Taiwan Warm Current and to the east is the Kuroshio. When the wind was southwesterly, the TWC and Kuroshio were stronger (Fig. 9a); when the wind reversed, both currents became weaker (Figs. 9b,c). The currents were weak on the northern shelf of Taiwan.

The right panels of Fig. 9 show R_o. Large positive and negative R_os, are seen, and they are primarily due to the strong shears of the Kuroshio and TWC on both sides of the upwelling region (left panel of Fig. 9) and are negative on the northern shelf of Taiwan. Spatial differences in relative vorticity produce variable Ekman transports according to Eq. (4), which then generate compensation flows below the surface layer (e.g., Fig. 4).

The direction of the surface Ekman transport is controlled by the wind stress. Ekman transport is eastward for southerly wind and westward for wind from the north. In Fig. 4b, the surface Ekman transport is westward and large over the northern shelf, where R_o is negative, and it is smaller for regions to the west (TWC) and east (Kuroshio), where R_o is positive. The subsurface water therefore upwells to the east and downwells to the west to compensate for the surface divergence and convergence, respectively. Surface Ekman transport along the track in August 2001 is estimated based on Eq. (4) (Fig. 10a). Colors separate positive (red; eastward) and negative values (blue; westward). During the northeasterly wind from 13 to 21 August, there was a strong westward Ekman transport near 121.4°–121.6°E (darker blue in Fig. 10a); the Ekman transport east of 121.6°E was weak, so upwelling occurred on the northern shelf of Taiwan east of 121.6°E (Figs. 8b,c). This idea can also

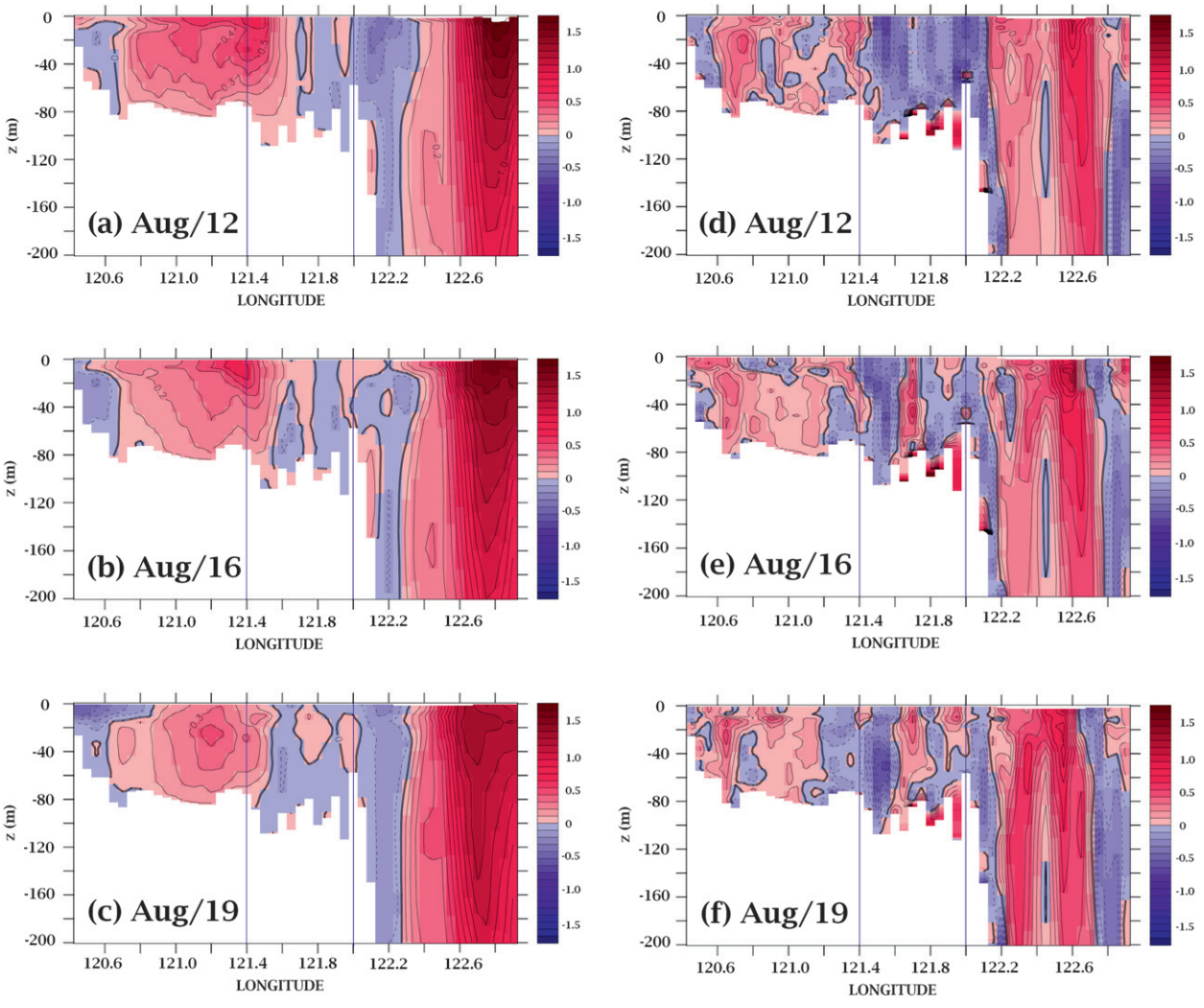

FIG. 9. Section contours of the (left) modeled normal-to-section velocity (positive northeastward) and (right) R_o along the track shown in Fig. 2 on (a),(d) 12 Aug; (b),(e) 16 Aug; and (c),(f) 19 Aug. The contour interval is 0.1 m s^{-1} for velocity and 0.1 for R_o.

explain the warm water from the surface to the depth of $z = -70$ m at approximately 121.6°E because of the downwelling on Aug 12 during an upwelling-favorable southwesterly wind (Fig. 7a). In this case, Fig. 10a shows that, from 4 to 8 August, the Ekman transport west of 121.6°E was strongly eastward (darker red). Thereafter, the wind weakened, and most of the downwelling and warming of water column therefore occurred prior to 12 August (Fig. 7a).

To assess the extent to which the simplified Eq. (4) applies in the numerical model, Fig. 10b shows the correlation coefficient (blue bars) along the track between the surface Ekman transport based on Eq. (4) and the modeled transport in the upper 15 m for August 2001. The black solid line indicates the 95% confidence level. The correlation is significant and exceeds 0.4–0.5 over most of the shelf including the western edge of the Kuroshio (near 122.2°~122.4°E), is weak near the axis of the Kuroshio, and increases again seaward. The vorticity effects show up as localized minima and maxima in Fig. 10a representing, for a northeasterly wind, surface divergence (convergence) east of a local minimum (maximum). As a further check, a smoothed (10-day running average) background time series representing an estimate of the large-scale Ekman transport is removed; the correlation decreases to 0.3–0.4 but is still significant. A repeated calculation using the vertical velocity yields a virtually identical result (see also Fig. 8). Given that the realistic model contains processes (eddies, topographic influences, etc.) other than wind-induced transports, the correlation indicates that Ekman divergence and convergence as a result of wind action on the vorticity field is a significant part of the circulation dynamics over the northern shelf of Taiwan.

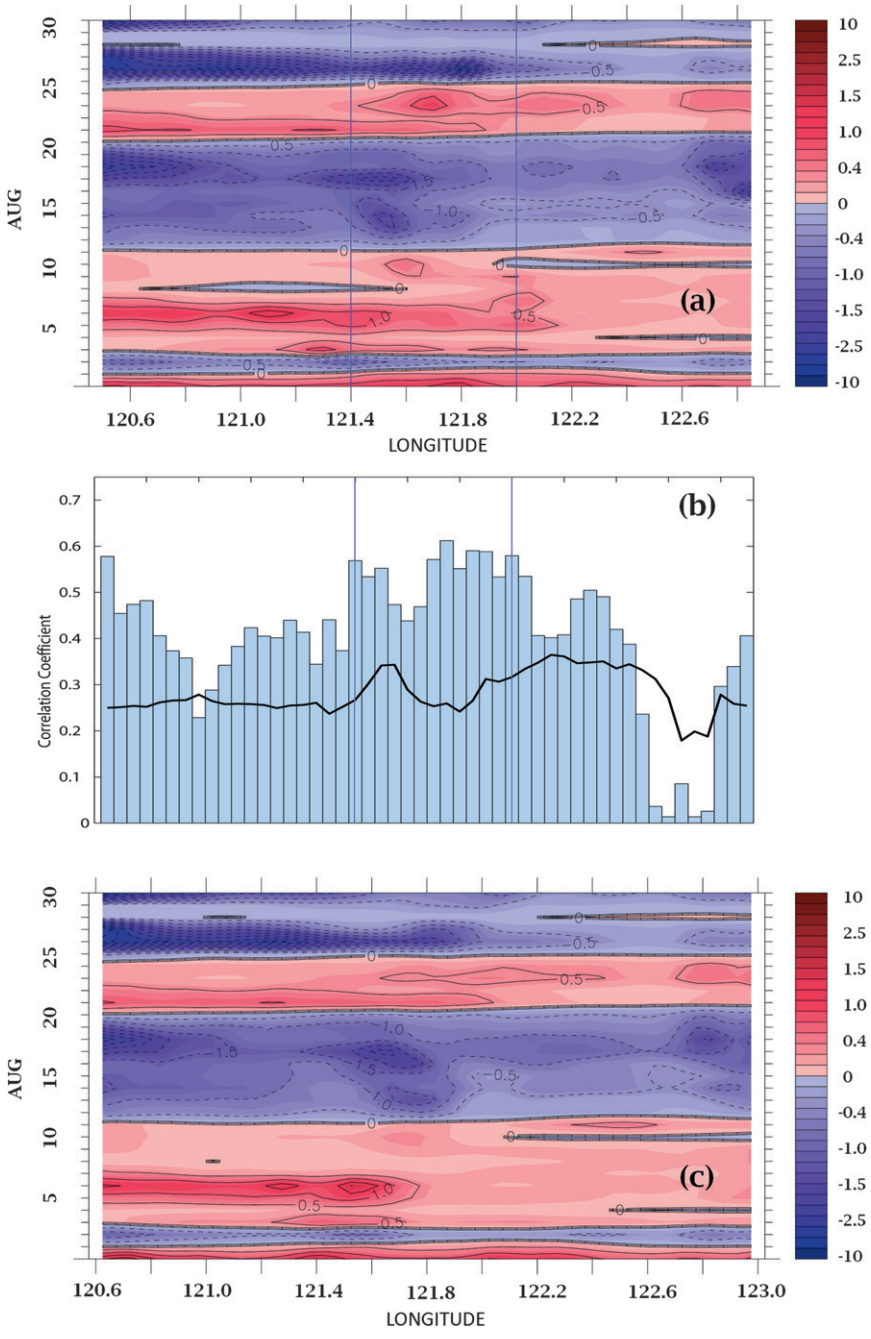

FIG. 10. (a) Along-track and time contours of (a) surface Ekman transport along the transect shown in Fig. 2. (b) Correlation coefficient (bars) between modeled transport in the upper 15 m and surface Ekman transport. The black line shows the 95% confidence level, and the vertical blue lines delineate the northern shelf region. (c) Surface Ekman transport of a more northern transect (see text). The contour interval is 0.5 m^2 s^{-1}.

The previous paragraph assumes that surface convergences and divergences are mainly controlled by cross-shelf (i.e., along transect) variations in the vorticity field. This appears to be true (Fig. 10b), even though the Chen and Wang transect is only about 25 km off the northern coast of Taiwan. As a further check, a more northern track (50 km farther north than the Chen and Wang transect shown in Figs. 2, 7–9, 10a,b) is chosen. The surface Ekman transport along this northern track is plotted in Fig. 10c, and it shows very similar

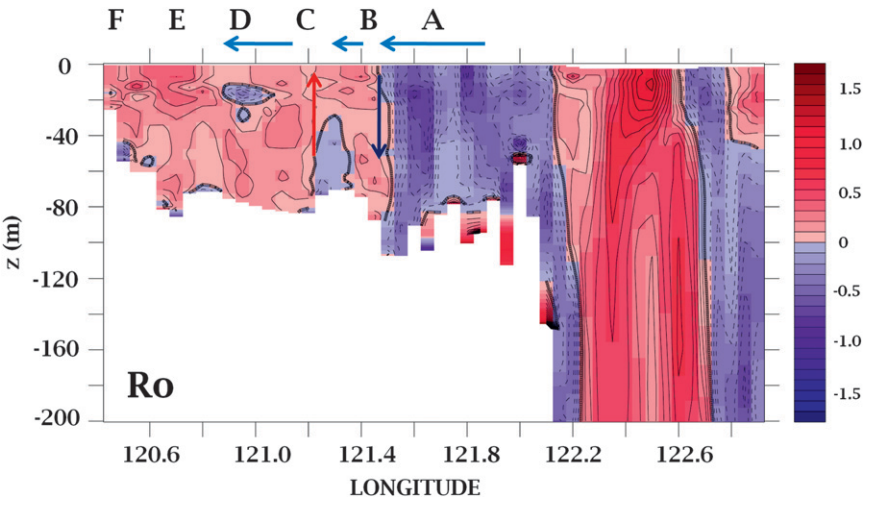

FIG. 11. Section contours of the nondimensional vorticity ζ/f_o averaged from 27 to 28 Aug 2001 during Chen and Wang's (2006) observation along the transect shown in Fig. 2. Arrows schematically indicate surface Ekman transports and compensating vertical flows.

convergences and divergences with those found along Chen and Wang's transect.

After the southwesterly wind event from 23 to 25 August, the wind turned northeasterly from 26 August. This downwelling-favorable wind period coincided with Chen and Wang's (2006) cruise period (27–28 August). Simulated temperature averaged over the cruise period (not shown) is similar to observation with vertically well-mixed water on the northern shelf of Taiwan near Chen and Wang's station A (their Fig. 5a; see also http://aos.princeton.edu/WWWPUBLIC/PROFS/PUBLICATION/chang_etal_jpo2010_CompareObsChenWang.pdf). Based on temperature, salinity, and nutrient analyses, Chen and Wang (2006) suggested that the well-mixed water came from downwelling water from offshore, which is then upwelled at station C. The R_o plot in Fig. 11 shows how these rather complex downwelling and upwelling patterns may be explained. The R_o was strongly negative near 121.6°E near station A, was positive near 121.4°E (station B), and then became weaker farther to the west near 121.2°E (station C). The surface Ekman transport was therefore strongly westward near A, reached a minimum near B, and became stronger to the west of C. The downwelling and upwelling patterns indicated in Fig. 11 agree well with Chen and Wang's analysis.

6. Conclusions

Upwellings were observed off the northern shelf of Taiwan in previous studies (Liu et al. 1992b; Wong et al. 2004; Chen and Wang 2006) during the onset of northeasterly monsoon wind. Temperature observations in August–September 2001 (this work) at a buoy located off the northeastern coast of Taiwan support these previous findings. The rate of change of SST correlates well with the wind, showing a cooling trend during northeasterly wind but a warming trend when the wind turned southwesterly. This cannot be explained by simple wind-driven Ekman advection $\approx -\tau_0^y/(f\delta_E)(\partial T_0/\partial x)$ [the first term on the rhs of Eq. (2b)], which would predict a temperature rise for northeasterly wind. Instead, Ekman divergences caused by spatial differences in the surface vorticity $\tau_0^y/(f\delta_E)(\partial\zeta_s/\partial x)\Delta T/f$ [the second term on the rhs of (2b)] is important; in fact, it appears to be dominant on the western portion of the Kuroshio over the shelf edge. A simple analytical model and a numerical model are used to illustrate this mechanism. We show that upwellings occurred on the northern shelf of Taiwan during northeasterly wind. The northern shelf of Taiwan is sandwiched between two strong fronts (Kuroshio and TWC); the corresponding vorticity (or R_o) was generally negative on the northern shelf of Taiwan and was strongly positive to the east and to the west. The spatial gradients in the vorticity filed give rise to nonlinear shelf response to wind. Our numerical model suggests that the TWC plays an important role in producing the vertical motions on the shelf observed by Chen and Wang (2006). Finally, as sketched in Fig. 4b, the fall–winter monsoon (northeasterly) wind would tend to upwell Kuroshio water over the shelf edge. The upwelled water is then deposited onto the shelf through surface convergence. This mechanism is robust because it depends only on wind and the presence of the Kuroshio and, on the shelf, the TWC as well. Missing in this description is the

effects of the bottom mixed layer, which should not be ignored, especially on the shelf. This will be the subject of a future paper.

Upwelling on the northern shelf of Taiwan appears to be a year-round phenomenon (Liu et al. 1992a). This persistency may suggest other upwelling mechanisms: for example, Kuroshio meanders and/or frontal eddies (e.g., Ito et al. 1995; Wu et al. 2008, and references therein). The study of these processes would require more complete observations in conjunction with finer-resolution numerical modeling. However, as pointed out by Liu et al. (1992b), ''The most dominant feature revealed by observations is the intensification of the upwelling center off northeast Taiwan shortly after the onset of the NE monsoon.'' The northeast monsoon is a distinct feature of the East Asian atmospheric variability. Over the East China Sea, long-term wind data (da Silva et al. 1994) show that northeasterly winds dominate, except in summer when weak southwesterly winds prevail (e.g., Fig. 3). Therefore, the proposed upwelling under northeasterly winds, which at times may be intensified over periods of days to weeks, is potentially an important mechanism for explaining the observed shelf-break upwelling, especially in nonsummer months.

Acknowledgments. We benefitted from comments from the two anonymous reviewers and the editor, Dr. Barth. YLC received a fellowship from the Graduate Student Study Abroad Program (NSC97-2917-I-003-103) of the National Science Council of Taiwan. CRW was supported by the National Science Council, Taiwan, ROC, under Grant NSC 98-2111-M-003-002-MY2.

REFERENCES

Chang, Y.-L., C.-R. Wu, and L.-Y. Oey, 2009: Bimodal behavior of the seasonal upwelling off the northeastern coast of Taiwan. *J. Geophys. Res.,* **114,** C03027, doi:10.1029/2008JC005131.

Chen, C. T. A., and S. L. Wang, 2006: A salinity front in the southern East China Sea separating the Chinese coastal and Taiwan Strait waters from Kuroshio waters. *Cont. Shelf Res.,* **26,** 1636–1653.

da Silva, A., A. C. Young, and S. Levitus, 1994: *Algorithms and Procedures*. Vol. 1, *Atlas of Surface Marine Data 1994,* NOAA Atlas NESDIS 6, 83 pp.

Hsin, Y.-C., C.-R. Wu, and P.-T. Shaw, 2008: Spatial and temporal variations of the Kuroshio east of Taiwan, 1982–2005: A numerical study. *J. Geophys. Res.,* **113,** C04002, doi:10.1029/2007JC004485.

Hsueh, Y., J. Wang, and C.-S. Chern, 1992: The intrusion of the Kuroshio across the continental shelf northeast of Taiwan. *J. Geophys. Res.,* **97,** 14 323–14 330.

Ito, T., A. Kaneko, H. Furukawa, N. Gohda, and W. Koterayama, 1995: A structure of the Kuroshio and its related upwelling on the East China Sea shelf slope. *J. Oceanogr.,* **51,** 267–278.

Large, W. G., and S. Pond, 1981: Open ocean momentum flux measurements in moderate to strong winds. *J. Phys. Oceanogr.,* **11,** 324–336.

Liang, W.-D., T. Y. Tang, Y. J. Yang, M. T. Ko, and W.-S. Chuang, 2003: Upper-ocean currents around Taiwan. *Deep-Sea Res. II,* **50,** 1085–1105.

Liu, K. K., G. C. Gong, S. Lin, C.-Y. Yang, C. L. Wei, S. C. Pai, and C. K. Wu, 1992a: The year-round upwelling at the shelf break near the northern tip of Taiwan as evidenced by chemical hydrography. *Terr. Atmos. Oceanic Sci.,* **3,** 243–276.

——, ——, C. Z. Shyu, S. C. Pai, C. L. Wei, and S. Y. Chao, 1992b: Response of Kuroshio upwelling to the onset of the northeast monsoon in the sea north of Taiwan: Observations and a numerical simulation. *J. Geophys. Res.,* **97,** 12 511–12 526.

Mellor, G. L., 2004: Users guide for a three-dimensional, primitive equation, numerical ocean model. Princeton University Program in Atmospheric and Oceanic Sciences, 56 pp.

——, and T. Yamada, 1982: Development of a turbulence closure model for geophysical fluid problems. *Rev. Geophys. Space Phys.,* **20,** 851–875.

Niiler, P. P., 1969: On the Ekman divergence in an oceanic jet. *J. Geophys. Res.,* **74,** 7048–7052.

Oey, L.-Y., Y.-C. Hsin, and C.-R. Wu, 2010: Why does the Kuroshio northeast of Taiwan shift shelfward in winter? *Ocean Dyn.,* **60,** 413–426.

Stern, M. E., and J. Austin, 1995: Entrainment of shelf water by a bifurcating continental boundary current. *J. Phys. Oceanogr.,* **25,** 3118–3131.

Thomas, L. N., and C. M. Lee, 2005: Intensification of oceanic fronts by down-front winds. *J. Phys. Oceanogr.,* **35,** 1086–1102.

Wang, Y. H., S. Jan, and D. P. Wang, 2003: Transports and tidal current estimates in the Taiwan Strait from shipboard ADCP observations (1999–2001). *Estuarine Coastal Shelf Sci.,* **57,** 193–199.

Wong, T. F. G., C.-C. Hung, and G.-C. Gong, 2004: Dissolved iodine species in the East China Sea—A complementary tracer for upwelling water on the shelf. *Cont. Shelf Res.,* **24,** 1465–1484.

Wu, C.-R., H.-F. Lu, and S.-Y. Chao, 2008: A numerical study on the formation of upwelling off northeast Taiwan. *J. Geophys. Res.,* **113,** C08025, doi:10.1029/2007JC004697.

Yanagi, T., T. Shimizu, and H.-J. Lie, 1998: Detailed structure of the Kuroshio frontal eddy along the shelf edge of the East China Sea. *Cont. Shelf Res.,* **18,** 1039–1056.